East European Journal of Physics. 1. 118-124 (2023)
DOI:10.26565/2312-4334-2023-1-14 ISSN 2312-4334

A QUALITATIVE THEORETICAL STUDY OF INORGANIC HTM-FREE $RbGeI_3$ BASED PEROVSKITE SOLAR CELLS USING SCAPS-1D AS A PATHWAY TOWARDS 3.601% EFFICIENCY†

Mary T. Ekwu[a], Eli Danladi[b], Nicholas N. Tasie[c], Idoko S. Haruna[d], Osaretin E. Okoro[d], Philibus M. Gyuk[e], Olayinka M. Jimoh[f], Rita C. Obasi[d]

[a]*Department of Physics, Airforce Institute of Technology, Kaduna, Nigeria*
[b]*Department of Physics, Federal University of Health Sciences, Otukpo, Benue State, Nigeria*
[c]*Department of Physics, Rivers State University, Port Harcourt, Rivers State, Nigeria*
[d]*Centre for Satellite Technology Development-NASRDA, Abuja, Nigeria*
[e]*Department of Physics, Kaduna State University, Kaduna, Nigeria*
[f]*Department of Physics, Federal University, Dutsin-Ma, Katsina State, Nigeria*
**Corresponding Author: danladielibako@gmail.com, tel.: +2348063307256*
Received January 20, 2023; revised January 28, 2023; accepted January 31, 2023

The presence of toxic lead in perovskite solar cells has hindered its commercial viability. In this present work, a mesoscopic inorganic lead-free perovskite solar cells based on $RbGeI_3$ was proposed and implemented using SCAPs simulation tool. The effect of electron transport material (ETM) and Absorber thickness were analyzed. When the device was first simulated, its power conversion efficiency (PCE), fill factor (FF), current density (J_{sc}), and open circuit voltage (V_{oc}) all reached values of 3.584% for PCE, 48.477% for FF, 25.385 mA/cm^2 for J_{sc}, and 0.291 V for V_{oc}. When the ETM and absorber are at their ideal thicknesses of 0.08 μm and 0.40 μm , the development of efficiency becomes stable. Using the aforementioned parameters, the optimized PSC device produced the following values: PCE = 3.601%, J_{sc} = 25.386 mA/cm^2, V_{oc} = 0.291 V, and FF = 48.637%. The PCE improvement over the basic device without optimization is around 1.01 times. The findings indicate that perovskite solar cell lacking HTM has a substantial capacity to absorb photon energy and produce electrons. It has also shown how to create environmentally clean and economically viable technology.
Keywords: *perovskite solar cells; $RbGeI_3$; SCAPS; layer thickness*
PACS: 41.20.Cv; 61.43.Bn; 68.55.ag; 68.55.jd; 73.25.+i; 72.80.Tm

1. INTRODUCTION

Organic-inorganic halide perovskites have attracted a lot of scientific interest due to their many benefits, such as their high coefficient of absorption, good solution processability, simplicity in synthesis, variable bandgap, and long diffusion length, to name just a few [1-3]. With a power conversion efficiency of 3.8%, Kojima et al. published the first study on their use in solar cells in 2009 [4].

In the past decade, a transformation in efficiency has risen to a value exceeding 25% [5-7]. However, the presence of toxic lead in perovskite absorber is considered as one of the major drawbacks towards its commercial viability. To carter for such problem, researchers have invested much efforts on other cations that are divalent among which are $Sn^{2+}$and Ge^{2+}, whose oxidation state is +2 and some of their properties close to that of lead [8].

$Sn^{2+}$and Ge^{2+} both have ionic radius smaller than Pb^{2+} with Sn^{2+} to be (1.35 Å), Ge^{2+} to be (0.73 Å) and Pb^{2+} to be (1.49 Å), so when Sn^{2+} and Ge^{2+} act as divalent cations to replace Pb^{2+}, it will not destroy the perovskite crystal structure [5, 9]. The ionic radius of Ge^{2+} is smaller than that of Sn^{2+} and Pb^{2+}, indicating that Ge-based perovskites have higher conductivity than Pb-based and Sn-based perovskites. Saikia et al. studied the effect of thickness, defect concentration, and dopant concentration on $CsGeI_3$-based PSCs [10]. Krishnamoorthy et al. fabricated $CsGeI_3$-based PSCs for the first time and achieved a PCE of 0.11%, which can be seen as a result of Ge^{2+} oxidation during fabrication [11]. Jayan and Sabastian [12] determined the optoelectronic, thermodynamic, structural, thermoelectric, and mechanical properties of $RbGeI_3$ perovskites as a function of various exchange correlations. Pindolia et al. investigated the effect of different hole transport materials (HTM) and electron transport materials (ETM) with $RbGeI_3$ as the light absorbing layer [5].

The instability in perovskite solar cells which is seen to result from organic compounds has been a major problem in the photovoltaic horizon [13, 14]. The commonly used HTM, Spiro-OMeTAD, involves a complex synthetic route with yields below 40% [5, 15, 16]. Organic charge transport materials become unstable under ambient conditions and light exposure [5, 17-20]. Devices without HTM are practical solutions to the problem of the expensive and unstable Spiro-OMeTAD that has limited the commercialization of PSCs technologies due to structural complexity, high cost, and poor stability. Etgar et al. created the first HTM-free PSC by using a Pb-based perovskite absorber as both a light harvester and a hole transport material at the same time [21]. To the best of our research knowledge, the utilization of $RbGeI_3$ as a perovskite absorber in a hole transport free structure has not been reported. In this research paper, an inorganic $RbGeI_3$ based PSC was investigated without HTM. The structure was proposed and implemented using SCAPS-1D software. By utilizing TiO_2 as ETM, fluorine doped tin oxide (FTO) as front contact and silver (Ag) as back contact, two layers'

† ***Cite as:*** M.T. Ekwu, E. Danladi, N.N. Tasie, I.S. Haruna, O.E. Okoro, P.M. Gyuk, O.M. Jimoh, and R.C. Obasi, East Eur. J. Phys. **1**, 118 (2023), https://doi.org/10.26565/2312-4334-2023-1-14
© M.T. Ekwu, E. Danladi, N.N. Tasie, I.S. Haruna, O.E. Okoro, P.M. Gyuk, O.M. Jimoh, R.C. Obasi, 2023

properties such as thickness of ETM and thickness of perovskite layer were optimized to obtain a PCE of 3.601%, FF of 48.637%, J_{sc} of 25.386 mA/cm^2 and V_{oc} of 0.291 V. The manuscript is categorized into four sections which include, the introduction, theoretical method & simulations, results and discussions and the conclusion part.

2. THEORETICAL METHODS AND DEVICE STRUCTURE

In this study, SCAPS-1D software version 3.3.10 was used to carry out the simulation. This software is based on basic semiconductor equations: the Poisson equation and the continuity equation of both charge carriers (holes and electrons) under steady-state condition [1].

The proposed device follows the configuration of FTO/TiO_2/$RbGeI_3$/Ag, which is depicted in Figure 1. Starting from illumination point, FTO is used as a front contact, ETL as TiO_2, the absorber layer as $RbGeI_3$ and silver (Ag) as the back contact. The front electrode's work function is 4.40 eV, whereas the counter electrode's work function is 4.63 eV. The simulation was run with an A.M. 1.5 spectrum light intensity (1000 W/m^2), a simulation temperature of 300 K, a simulation frequency of 1×10^{16} Hz, and a scanning voltage range of 0 to 1.40 V. Tables 1 and 2 summarized the information for each layer and the interface settings.

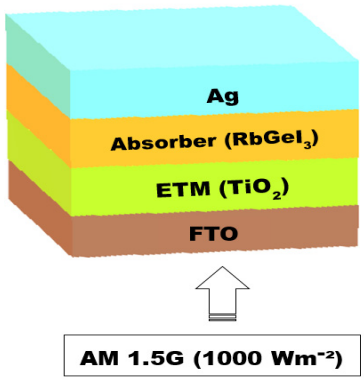

Figure 1. Device structure

Table 1. Variables utilized in SCAPS-1D simulations of perovskite solar cell architecture [1, 2, 5]

Parameters	FTO	TiO_2	$RbGeI_3$
Thickness (μm)	0.4	0.05	0.4
Band gap energy E_g (eV)	3.5	3.2	1.31
Electron affinity χ (eV)	4.3	4.2	3.9
Relative permittivity ϵ_r	9	10	23.01
Effective conduction band density N_c (cm^{-3})	2.2×10^{18}	2.2×10^{18}	2.8×10^{19}
Effective valance band density N_v (cm^{-3})	1.8×10^{19}	2.2×10^{18}	1.4×10^{19}
Electron thermal velocity (cm/s)	1.0×10^{7}	1.0×10^{7}	1.0×10^{7}
Hole thermal velocity (cm/s)	1.0×10^{7}	1.0×10^{7}	1.0×10^{7}
Electron mobility μ_n (cm^2 V^{-1} s^{-1})	20	20	28.6
Hole mobility μ_p (cm^2 V^{-1} s^{-1})	10	10	27.3
Donor concentration N_D (cm^{-3})	1.0×10^{18}	1×10^{17}	0
Acceptor concentration N_A (cm^{-3})	0	0	1×10^{9}
Defect density N_t (cm^{-3})	1×10^{15}	1×10^{15}	1×10^{15}

Table 2. Defect parameter values of the interfaces of the device

Parameters	TiO_2/$RbGeI_3$ interface
Defect type	Neutral
Capture cross section for electrons (cm^2)	1×10^{-18}
Capture cross section for holes (cm^2)	1×10^{-16}
Energetic distribution	Single
Energy level with respect to E_v (eV)	0.600
Characteristic energy (eV)	0.1
Total density (cm^{-3})	1×10^{12}

3. RESULTS AND DISCUSSIONS

3.1. Initial simulation

In accordance to the parameters presented in Tables 1 and 2, the initial device characteristics are shown in Figure 2. Figure 2a shows the current density-voltage (*J-V*) curve, Figure 2b shows the quantum efficiency (QE) curve with respect to wavelength, Figure 2c shows the quantum efficiency curve with respect to photon energy and Figure 2d shows the calculated energy band diagram profile. In this initial simulation, we ignored the reflection of each layer, as well as the interface and the additional series resistance brought on by front contact or back contact.

The incidence to photon conversion efficiency curve with respect to wavelength is shown in Figure 2b for the initial device. Based on the given curve in Figure 2c, the band gap energy of $RbGeI_3$ is 1.31 eV, which is narrower than the lead-based counter part of 1.55 eV, and this results to a red shift in the absorption wavelength of the lead-free perovskite absorber to 900 nm. The curve sweeps across the visible range of the electromagnetic spectrum, and the absorption from 380 to 780 nm is the strongest, seen above 78%, which is in good agreement with the QE spectrum in similar literature [5].

Based on the values listed in Tables 1 and 2, the band gap profile was calculated and is shown in Figure 2d. The highest energy level of the valence band is represented by E_v (eV), and the lowest energy level of the conduction band is represented by E_c (eV). The offset energy of the valance band is 2.186 eV while the interface conduction band offset is 0.319 eV. The offset value existing between valance band of $RbGeI_3$ and ETL prevents the positive charges from flowing to the TiO_2 side from the absorber layer whereas the offset value at their conduction band blocks the electron from diffusing to the absorber from the TiO_2. Thus, the recombination processes at the interface are minimal thereby resulting to good photovoltaic performance.

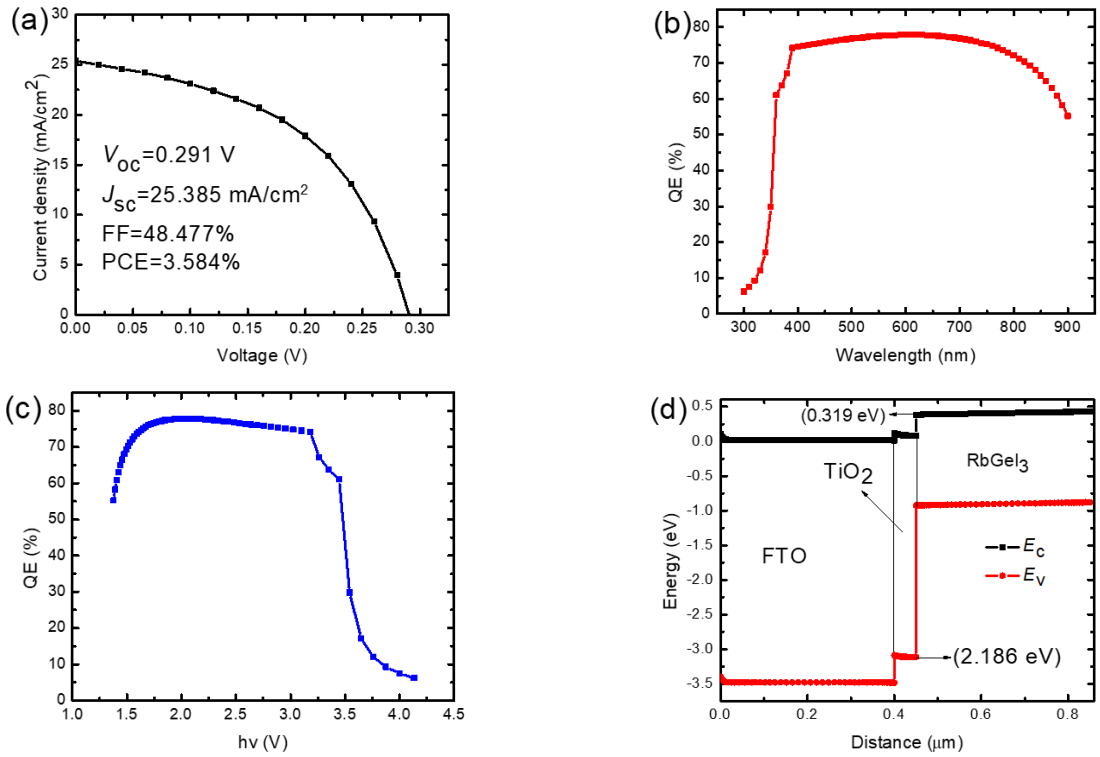

Figure 2. (a) *J-V* curve under illumination for initial device, (b) QE versus wavelength for initial device, (c) QE versus photon energy for the initial device and (d) energy profile diagram of the initial device

3.2. Effect of changing ETM thickness

To understand the influence of ETM thickness on PCE of the proposed PSC, we utilized the parameters in Tables 1 & 2 for the simulation while varying the thickness from 10 to 100 nm. The results are presented in Table 3 and Figure 3. The quantum efficiency versus wavelength curve is depicted in Figure 3b. The simulated results of our study show that PCE increased with increasing TiO_2 thickness from 10 to 80 nm before it starts decreasing. This decrease is attributed to lower transmittance at excessive values of ETM thickness that prohibit solar radiation from reaching the perovskite skeleton and partial TiO_2 layer absorption of incident light [1]. From Table 3 and Figure 3a, it can be seen that the 80 nm thickness gave V_{oc} = 0.291 V, J_{sc} = 25.385 mA/cm^2, FF = 48.637%, and PCE = 3.598%.

Table 3. *J-V* characteristic parameters with the variation of thickness of ETM

Thickness (μm)	PCE (%)	*FF* (%)	J_{sc} (mA/cm^2)	V_{oc} (V)
0.01	3.195	44.885	21.981	0.285
0.02	3.370	46.486	25.106	0.289
0.03	3.499	47.689	25.260	0.290
0.04	3.560	48.248	25.349	0.291
0.05	3.584	48.477	25.385	0.291
0.06	3.594	48.576	25.394	0.291
0.07	3.597	48.618	25.392	0.291
0.08	3.598	48.637	25.385	0.291
0.09	3.597	48.645	25.377	0.291
0.10	3.596	48.649	25.367	0.291

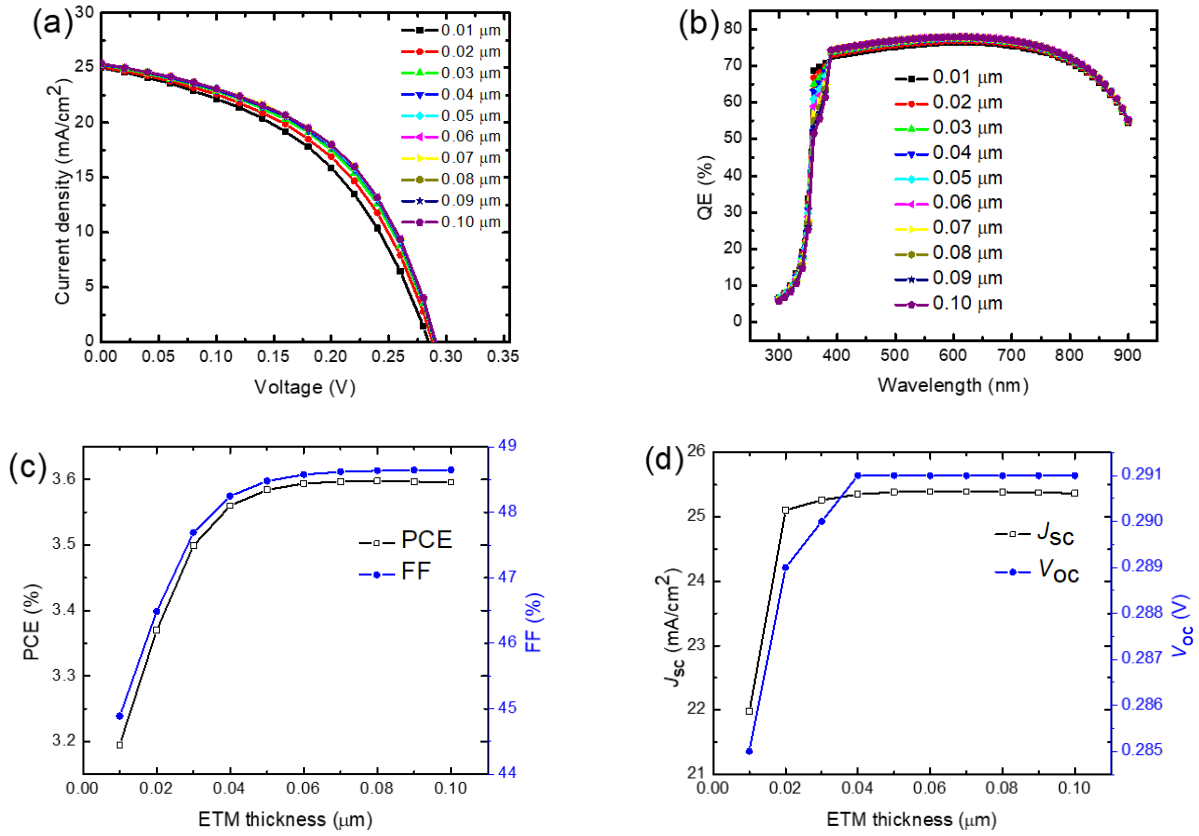

Figure 3. (a) *J-V* curve under illumination with different ETM thickness, (b) QE versus wavelength, (c) variation of ETM thickness with PCE and FF, and (c) variation of ETM thickness with J_{sc} and V_{oc}

The QE is a crucial property of solar cell, which shows the ratio of the electron–hole pairs collected to the number of striking photons [2]. QE is seen as a function of wavelength in nm or photon energy in eV. The curve was measured within the wavelength range of 300-900 nm. The simulated QE increased from 5% at 300 nm to a maximum of 78% at 600 nm but gradually decreases to 60% at a wavelength value of 900 nm. The absorption is within the visible and near infrared region. The correlation between the PCE and FF with respect to thickness is shown in Figure 3c and the relationship between J_{sc} and V_{oc} with thickness is shown in Figure 3d.

3.3. Effect of changing absorber layer thickness

One of the important parameters that should not be overlooked in choice for good device performance is the perovskite layer thickness. This thickness is affected by the diffusion lengths and life-time of the photo-generated electrons and holes [22, 23], as such should be properly chosen. For its influence in solar cells to be fully explored, the layer thickness was controlled in the range of 100–1000 nm while maintaining other parameters fixed as shown in Tables 1 & 2.

Figure 4a shows the *J-V* curves of the simulated device with varied $RbGeI_3$ layer thicknesses. As can be seen from the curve, when the absorber layer is increased, the J_{sc} increases significantly upto thickness of 500 nm, after which the J_{sc} value tends to have a downward trend as the absorbing layer thickness keeps increasing, which shows that absorber layer exceeding 500 nm encourages charge recombination. This rise in J_{sc} is due to a significant photon absorption in this range (as seen by the QE-wavelength curve). Along with the increase in absorber layer thickness from 100 to 400 nm, we also observed a rise in PCE. The thicker perovskite layer absorbs enough photons to produce charge carriers when the absorption layer thickness of the perovskite layer rises above 400 nm.

The PCE curve, however, tends to become flatter as absorption layer thickness increases due to increased recombination and diffusion length. The carriers may recombine before reaching the metal electrode if the thickness of the absorption layer is greater than the diffusion length of the carrier [22].

The research above determined the ideal value for the thickness of the absorber layer used for additional simulation and taken into account to be 400 nm (see Table 4). Due to a rise in series resistance, the value of FF as a function of absorber layer thickness decreases [22].

The impact of the $RbGeI_3$ layer's thickness on the QE (%) with respect to wavelength is depicted in Figure 4b. Since the absorption grows more potent and quantum efficiency also rises with thickness, carrier extraction rises along with thickness. Figure 4c displays the relationship between the PCE and FF with regard to thickness, whereas Figure 4d displays the relationship between the J_{sc} and V_{oc} with respect to thickness.

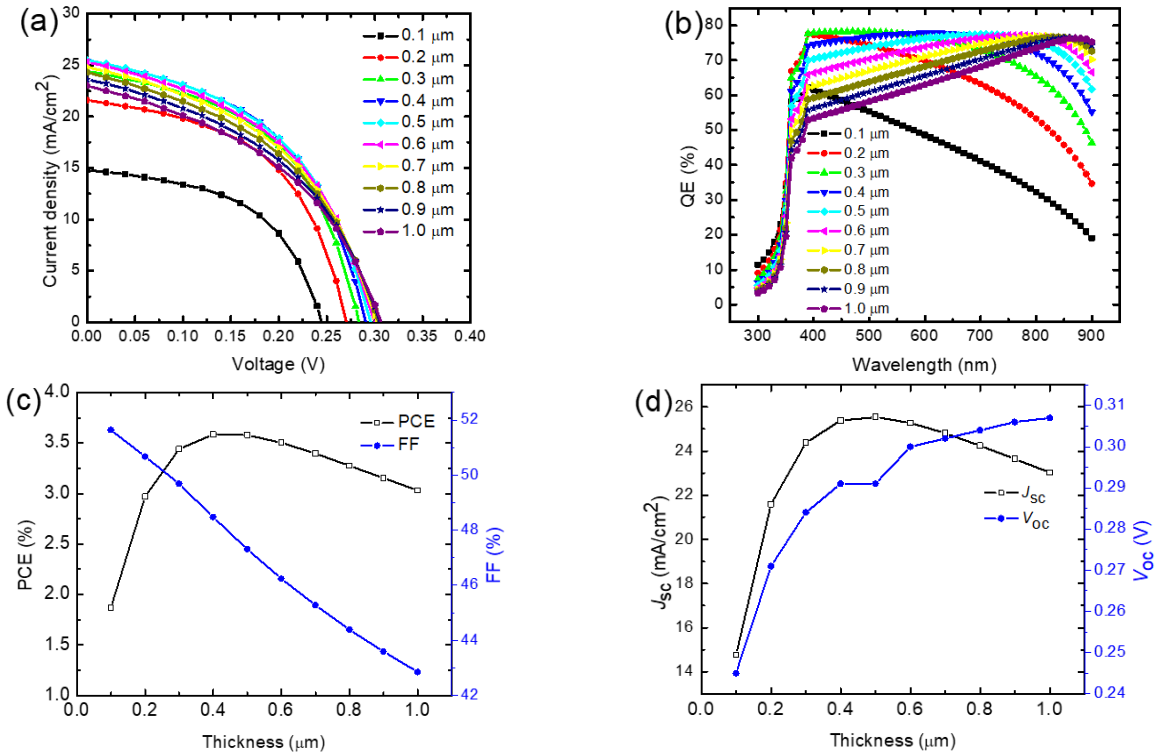

Figure 4. (a) *J-V* curve under illumination with different absorber thickness, and (b) QE versus wavelength, (c) variation of ETM thickness with PCE and FF, and (d) variation of ETM thickness with J_{sc} and V_{oc}

Table 4. *J-V* characteristic parameters with the variation of thickness of Absorber

Thickness (μm)	PCE (%)	*FF* (%)	J_{sc} (mA/cm^2)	V_{oc} (V)
0.1	1.870	51.638	14.767	0.245
0.2	2.969	50.677	21.594	0.271
0.3	3.440	49.687	24.384	0.284
0.4	3.584	48.477	25.385	0.291
0.5	3.579	47.311	25.541	0.291
0.6	3.503	46.239	25.282	0.300
0.7	3.396	45.279	24.815	0.302
0.8	3.274	44.387	24.251	0.304
0.9	3.152	43.593	23.646	0.306
1.0	3.030	42.853	23.029	0.307

3.4. Performance of the optimized device

Figure 5 shows the curve of the optimized (black color) and initial (red color) device. The optimized ETM thickness is 80 nm while the optimized $RbGeI_3$ layer thickness is 400 nm.

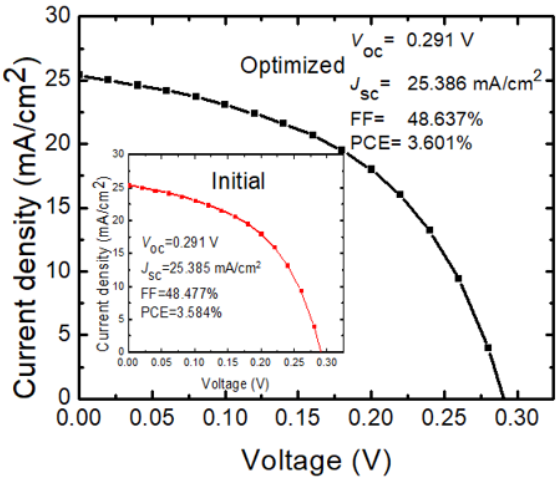

Figure 5. The initial and optimized *J–V* curves

The optimized device gave a PCE of 3.601%, J_{sc} of 25.386 mA/cm^2, V_{oc} of 0.291 V, and FF of 48.637%. This shows an improvement of ~ 1.01 times in PCE over the initial device without optimization. The results obtained demonstrate that, ETM and absorber thickness have crucial role in improving the performance of $RbGeI_3$ HTM free perovskite solar cell. This can provide proper guidance to researchers involved in experimental development of perovskite solar cells for realizing high performance.

3.5. Influence of temperature on the performance of the optimized PSC device

To explore the properties of the optimized device, we simulated the device at different temperature which include 240, 250, 260, 270, 280, 290, 300, 310 and 320 K. Figure 6a depicts the *J-V* behavior, while Figures 6b-f show the power density with the changing temperature, variation of the PCE

with the temperature, correlation of the FF with respect to the temperature, variation of J_{sc} with the temperature and correlation of the V_{oc} with respect to the temperature. The performance of the device is significantly impacted by temperature changes, as can be readily shown in Table 5. With an increase in temperature, the V_{oc}, J_{sc}, and PCE continuously decrease. The increase in saturation current, which also causes an increase in recombination rate, is responsible for these observed properties [24]. Low PCE and J_{sc} are a result of recombination, which has an impact on the carrier concentration, electron and hole mobilities, and the ability of the electron to reach the depletion area [1, 2]. The increase in flaws with rising temperature is thought to be the cause of the observed drop in V_{oc}.

Table 5. *J-V* characteristic parameters with temperature variation

Temperature (K)	PCE (%)	*FF* (%)	J_{sc} (mA/cm^2)	V_{oc} (V)
240	4.674	48.047	26.776	0.363
250	4.511	47.782	26.558	0.355
260	4.335	47.597	26.337	0.346
270	4.160	47.650	26.112	0.334
280	3.992	47.991	25.885	0.321
290	3.787	48.099	25.655	0.307
300	3.601	48.637	25.386	0.291
310	3.363	48.537	25.178	0.275
320	3.152	48.906	24.933	0.258

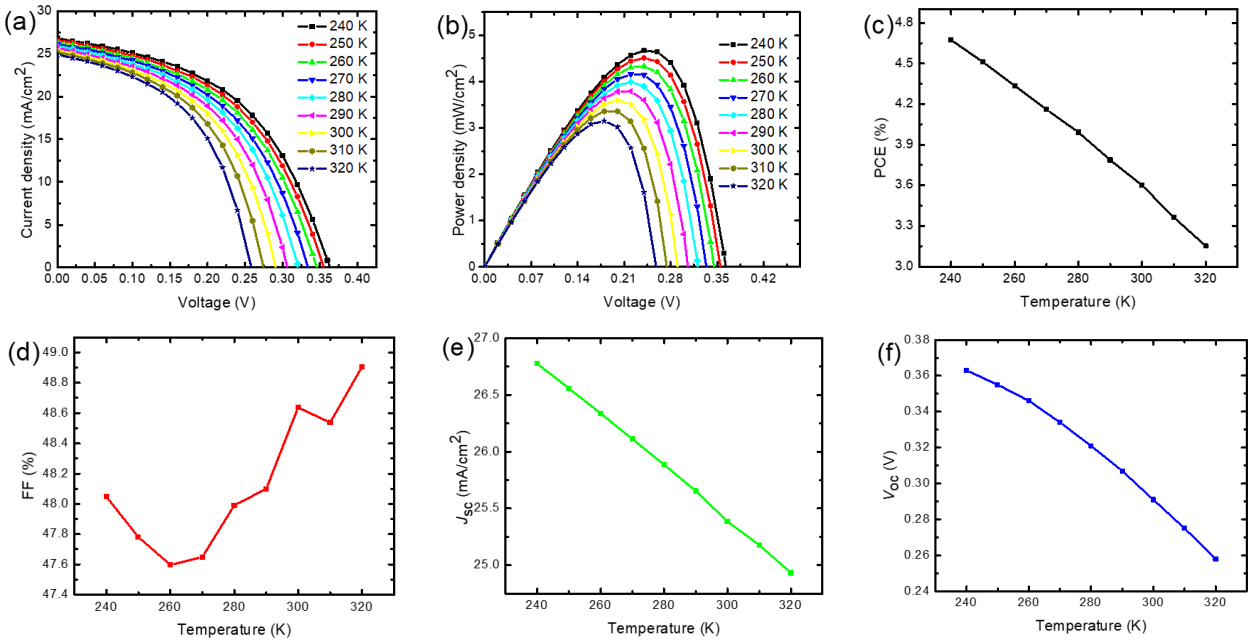

Figure 6. (a) *J-V* curve with varied temperature under illumination, (b) *P-V* curve with varied temperature under illumination (c) PCE with respect to temperature, (d) FF with respect to temperature, (e) J_{sc} with respect to temperature and (f) V_{oc} with respect to temperature

4. CONCLUSION

We utilized SCAPS software which is based on the three basic equations of semiconductor to simulate the proposed HTM-free $RbGeI_3$ PSC structure. On initial device simulation, its power conversion efficiency, fill factor, current density and open circuit voltage attained values of 3.584%, 48.477%, 25.385 mA/cm^2 and 0.291 V. For the solar cell device to be optimized, the ETM and $RbGeI_3$ thicknesses were varied individually from 10 to 100 nm and from 100 to 1000 nm while keeping other parameters fixed. The optimized thickness of ETM was 80 nm and the optimized thickness of $RbGeI_3$ was 400 nm. The optimized PSC device using the aforementioned parameters gave a PCE of 3.601%, J_{sc} of 25.386 mA/cm^2, V_{oc} of 0.291 V, and FF of 48.637% respectively. The performance of the optimized device is greatly affected by the temperature. Increase in temperature leads to decrease in PCE, J_{sc} and V_{oc}.

Acknowledgement

The authors would like to thank Professor Marc Burgelman, Department of Electronics and Information Systems, University of Ghent for the development of the SCAPS software package and allowing its use.

Funding. This article did not receive any funding support.
Conflict of interest. Authors have declared that there is no conflict of interest.

ORCID IDs

Eli Danladi, https://orcid.org/0000-0001-5109-4690; **Nicholas N. Tasie**, https://orcid.org/0000-0001-8398-2596

REFERENCES

[1] E. Danladi, M. Kashif, A. Ichoja, and B.B. Ayiya, Transactions of Tianjin University, **28**(5), (2022). https://doi.org/10.1007/s12209-022-00343-w
[2] E. Danladi, M. Kashif, T.O Daniel, C.U. Achem, M. Alpha, and M. Gyan, East European Journal of Physics, **3**, 19 (2022). https://doi.org/10.26565/2312-4334-2022-3-03
[3] Z. Qu, F. Ma, Y. Zhao, X. Chu, S. Yu, and J. You, Chinese Physics Letters, **38**, 107801 (2021). https://doi.org/10.1088/0256-307X/38/10/107801
[4] A. Kojima, K. Teshima, Y. Shirai, and T. Miyasaka, Journal of American Chemical Society, **131**, 6050 (2009). https://doi.org/10.1021/ja809598r
[5] G. Pindolia, S.M. Shinde, P.K. Jha, Solar Energy, **236**, 802 (2022). https://doi.org/10.1016/j.solener.2022.03.053
[6] J. Wu, Y. Li, Y. Li, W. Xie, J. Shi, D. Li, S. Cheng, and Q. Meng, Journal of Materials Chemistry A, **9**, 6382 (2021). https://doi.org/10.1039/D0TA12046D
[7] J.J. Yoo, G. Seo, M.R. Chua, T.G. Park, Y. Lu, F. Rotermund, Y.K. Kim, et al., Nature, **590**(7847), 587 (2021). https://doi.org/10.1038/s41586-021-03285-w
[8] W. Ke, and M.G. Kanatzidis, Nature Communications, **10**, 965 (2019). https://doi.org/10.1038/s41467-019-08918-3
[9] N.K. Noel, S.D. Stranks, A. Abate, C. Wehrenfennig, S. Guarnera, A.A. Haghighirad, A. Sadhanala, G.E. Eperon, S.K. Pathak, M.B. Johnston, A. Petrozza, L.M. Herz, and H.J. Snaith, Energy & Environmental Science, **7**, 3061 (2014). https://doi.org/10.1039/C4EE01076K
[10] D. Saikia, J. Bera, A. Betal, and S. Sahu, Optical Materials, **123**, 111839 (2022). https://doi.org/10.1016/j.optmat.2021.111839
[11] T. Krishnamoorthy, H. Ding, C. Yan, W.L. Leong, T. Baikie, Z. Zhang, M. Sherburne, S. Li, M. Asta, N. Mathews, and S.G. Mhaisalkar, Journal of Materials Chemistry A, **3**, 23829 (2015). https://doi.org/10.1039/C5TA05741H
[12] D.K. Jayan, and V. Sebastian, Materials Today Communications, **28**, 102650 (2021). https://doi.org/10.1016/j.mtcomm.2021.102650
[13] M.G. Ju, M. Chen, Y. Zhou, J. Dai, L. Ma, N.P. Padture, and X.C. Zeng, Joule, **2**, 1231 (2018). https://www.cell.com/joule/pdf/S2542-4351(18)30187-9.pdf
[14] T. Leijtens, G.E. Eperon, N.K. Noel, S.N. Habisreutinger, A. Petrozza, and H.J. Snaith, Advanced Energy Materials, **5**(20), 1500963 (2015). https://doi.org/10.1002/aenm.201500963
[15] T.P.I. Saragi, T. Spehr, A. Siebert, T. Fuhrmann-Lieker, and J. Salbeck, Chemical Reviews, **107**, 1011 (2007). https://doi.org/10.1021/cr0501341
[16] J.M. Tour, R. Wu, and J.S. Schumm, Journal of the American Chemical Society, **112**, 5662 (1990). https://doi.org/10.1021/ja00170a053
[17] A.F. Akbulatov, L.A. Frolova, M.P. Griffin, I.R. Gearba, A. Dolocan, D.A. Vanden Bout, S. Tsarev, E.A. Katz, A.F. Shestakov, K.J. Stevenson, and P.A. Troshin, Advanced Energy Materials, **7**, 1700476 (2017). https://doi.org/10.1002/aenm.201700476
[18] Z. Hawash, L.K. Ono, S.R. Raga, M.V. Lee, and Y. Qi, Chemistry of Materials, **27**, 562 (2015). https://doi.org/10.1021/cm504022q
[19] A.K. Jena, Y. Numata, M. Ikegami, and T. Miyasaka, Journal of Materials Chemistry A, **6**, 2219 (2018). https://doi.org/10.1039/C7TA07674F
[20] K. Norrman, M.V. Madsen, S.A. Gevorgyan, and F.C. Krebs, Journal of the American Chemical Society, **132**, 16883 (2010). https://doi.org/10.1021/ja106299g
[21] L. Etgar, P. Gao Z. Xue, Q. Peng, A.K. Chandiran, B. Liu, M.K. Nazeeruddin, and M. Gratzel, Journal of the American Chemical Society, **134**(42), 17396 (2012). https://doi.org/10.1021/ja307789s
[22] M.O. Abdulmalik, E. Danladi, R.C. Obasi, P.M. Gyuk, F.U. Salifu, S. Magaji, A.C. Egbugha, and D. Thomas, East European Journal of Physics, 4, 125 (2022). https://periodicals.karazin.ua/eejp/article/view/20949
[23] J. Barb´e, M.L. Tietze, M. Neophytou, B. Murali, E. Alarousu, A. el Labban, M. Abulikemu, W. Yue, O.F. Mohammed, I. McCulloch, A. Amassian, and S. del Gobbo, ACS Applied Materials Interfaces, **9**, 11828 (2017). https://doi.org/10.1021/acsami.6b13675
[24] S. Ahmed, F. Jannat, M.A.K. Khan, and M.A. Alim, Optik, **225**, 165765 (2021). https://doi.org/10.1016/j.ijleo.2020.165765

ЯКІСНЕ ТЕОРЕТИЧНЕ ДОСЛІДЖЕННЯ НЕОРГАНІЧНИХ СОНЯЧНИХ ЕЛЕМЕНТІВ НА ОСНОВІ ПЕРОВСКІТУ, БЕЗ HTM $RbGeI_3$, З ВИКОРИСТАННЯМ SCAPS-1D ЯК ШЛЯХУ ДО 3,601% ЕФЕКТИВНОСТІ

Мері Т. Екву[a], Елі Данладі[b], Ніколас Н. Таці[c], Ідоко С. Харуна[d], Осаретін Е. Окоро[d], Філібус М. Гюк[e], Олаїнка М. Джімо[f], Ріта К. Обасі[d]

[a]*Факультет фізики, Технологічний інститут ВПС, Кадуна, Нігерія*
[b]*Факультет фізики, Федеральний університет наук про здоров'я, Отукпо, штат Бенуе, Нігерія*
[c]*Факультет фізики, Університет штату Ріверс, Порт-Гаркорт, штат Ріверс, Нігерія*
[d]*Центр розвитку супутникових технологій NASRDA, Абуджа, Нігерія*
[e]*Факультет фізики, Університет штату Кадуна, Кадуна, Нігерія*
[f]*Факультет фізики, Федеральний університет, Дутсін-Ма, штат Каціна, Нігерія*

Наявність токсичного свинцю в перовскітних сонячних елементах перешкоджає їх комерційній життєздатності. У цій роботі було запропоновано та реалізовано мезоскопічні неорганічні безсвинцеві перовскітні сонячні батареї на основі RbGeI3 за допомогою інструменту моделювання SCAP. Було проаналізовано вплив матеріалу транспортування електронів (ETM) і товщини поглинача. Коли пристрій було вперше змодельовано, його ефективність перетворення потужності (PCE), коефіцієнт заповнення (FF), щільність струму (J_{sc}) і напруга холостого ходу (V_{oc}) досягали значень 3,584%, 48,477% для коефіцієнта заповнення, 25,385 мА/см^2 для J_{sc} і 0,291 В для V_{oc}. Коли ETM і абсорбер мають ідеальну товщину 0,08 і 0,40, розвиток ефективності стає стабільним. Використовуючи вищезазначені параметри, оптимізований пристрій PSC дав такі значення: PCE = 3,601%, J_{sc} = 25,386 мА/см^2, V_{oc} = 0,291 В і FF = 48,637%. Покращення PCE порівняно з базовим пристроєм без оптимізації становить приблизно 1,01 рази. Отримані дані показують, що перовскітний сонячний елемент без HTM має значну здатність поглинати енергію фотонів і виробляти електрони. Він також показав, як створити екологічно чисту та економічно життєздатну технологію.

Ключові слова: *перовскітні сонячні елементи; $RbGeI_3$; SCAPS; товщина шару*